Transspinal direct current stimulation immediately modifies motor cortex sensorimotor maps

Article *in* Journal of Neurophysiology · February 2015

DOI: 10.1152/jn.00784.2014 · Source: PubMed

4 authors, including:

Dennis Truong
City College of New York
72 PUBLICATIONS **1,062** CITATIONS
SEE PROFILE

Marom Bikson
City College of New York
415 PUBLICATIONS **11,897** CITATIONS
SEE PROFILE

John H Martin
City College of New York
95 PUBLICATIONS **3,139** CITATIONS
SEE PROFILE

J Neurophysiol 113: 2801–2811, 2015.
First published February 11, 2015; doi:10.1152/jn.00784.2014.

Transspinal direct current stimulation immediately modifies motor cortex sensorimotor maps

Weiguo Song,[1] Dennis Q. Truong,[2] Marom Bikson,[2] and John H. Martin[1,3]

[1]*Department of Physiology, Pharmacology and Neuroscience, City College of the City University of New York, New York, New York;* [2]*Department of Biomedical Engineering, City College of the City University of New York, New York, New York; and* [3]*Graduate Center of the City University of New York, New York, New York*

Submitted 6 October 2014; accepted in final form 6 February 2015

Song W, Truong DQ, Bikson M, Martin JH. Transspinal direct current stimulation immediately modifies motor cortex sensorimotor maps. *J Neurophysiol* 113: 2801–2811, 2015. First published February 11, 2015; doi:10.1152/jn.00784.2014.—Motor cortex (MCX) motor representation reorganization occurs after injury, learning, and different long-term stimulation paradigms. The neuromodulatory approach of transspinal direct current stimulation (tsDCS) has been used to promote evoked cortical motor responses. In the present study, we used cathodal tsDCS (c-tsDCS) of the rat cervical cord to determine if spinal cord activation can modify the MCX forelimb motor map. We used a finite-element method model based on coregistered high-resolution rat MRI and microcomputed tomography imaging data to predict spinal current density to target stimulation to the caudal cervical enlargement. We examined the effects of cathodal and anodal tsDCS on the H-reflex and c-tsDCS on responses evoked by intracortical microstimulation (ICMS). To determine if cervical c-tsDCS also modified MCX somatic sensory processing, we examined sensory evoked potentials (SEPs) produced by wrist electrical stimulation and induced changes in ongoing activity. Cervical c-tsDCS enhanced the H-reflex, and anodal depressed the H-reflex. Using cathodal stimulation to examine cortical effects, we found that cervical c-tsDCS immediately modified the forelimb MCX motor map, with decreased thresholds and an expanded area. c-tsDCS also increased SEP amplitude in the MCX. The magnitude of changes produced by c-tsDCS were greater on the motor than sensory response. Cervical c-tsDCS more strongly enhanced forelimb than hindlimb motor representation and had no effect on vibrissal representation. The finite-element model indicated current density localized to caudal cervical segments, informing forelimb motor selectivity. Our results suggest that c-tsDCS augments spinal excitability in a spatially selective manner and may improve voluntary motor function through MCX representational plasticity.

motor cortex; movement control; neuromodulation; rehabilitation; spinal cord

TRANSCRANIAL direct current (DC) stimulation (tDCS) modulates cortical excitability (Alonzo et al. 2012; Cambiaghi et al. 2010; Nitsche and Paulus 2000) and has been used to treat neurological and psychiatric disorders (da Silva et al. 2013; Nitsche et al. 2009; Shiozawa et al. 2013) as well as to improve motor learning (Javadi et al. 2012). A newer, related technique, transcutaneous spinal DC stimulation (tsDCS), modulates motor output in a polarity-dependent manner at the lumbar spinal cord (Ahmed 2011). tsDCS has been used to amplify corticospinal tract (CST) output in a mouse model (Ahmed 2013b). Because tsDCS can be implemented as a noninvasive neuromodulatory method in humans, it is promising for motor neurorehabilitation after stroke or spinal cord injury. However, translation to a robust clinical tool requires the characterization of systems-level mechanisms by which stimulation is acting to modify motor output.

In the present study, we examined the capacity of tsDCS to modify the motor cortex (MCX) motor map. The MCX motor map is plastic throughout life and, importantly, is thought to represent the capacity for skilled voluntary movement control (Monfils et al. 2005). The size of the representation of the different joints/limb is closely associated with skilled motor function, increasing with training and decreasing with disuse (Kleim et al. 1998). We hypothesized that tsDCS could modify the motor map through its action to increase the excitability of local spinal circuits. However, motor map plasticity produced by tsDCS could also reflect changes in spinal somatic sensory processing, as recently shown (Aguilar et al. 2011), which, in turn, could affect the motor representation (Jiang et al. 2013).

The focus of this study was to determine the effect of cathodal tsDCS (c-tsDCS) of the cervical spinal cord on the plasticity of the MCX forelimb motor map with intracortical microstimulation (ICMS). We chose c-tsDCS both because of the effects on spinal reflex function and our preliminary findings (Song and Martin 2013) as well as findings in the mouse (Ahmed 2011). We also examined the effect on the MCX somatic sensory map using sensory evoked potentials (SEPs) and changes in ongoing MCX network activity. We used a finite-element method (FEM) computational model to predicate the regional current density and electric field in the spinal cord during c-tsDCS. The results of the model determined optimal electrode placement for stimulation of the cervical enlargement. It is well known that DC modulation of neural function produces robust effects after the cessation of stimulation [i.e., aftereffects (Nitsche and Paulus 2000)]. In the present study, we tested the effects of c-tsDCS during stimulation to directly assess the effect of induced excitability changes of DC stimulation on the plasticity of sensorimotor maps. This enabled study of induced excitability changes without concurrent changes in the anesthesia level. To assess the specificity of cervical spinal stimulation on motor output, we compared the effects on the forelimb MCX motor map with those for the hindlimb and vibrissae.

We showed that cervical c-tsDCS enhanced the H-reflex and increased forelimb movement representation in the MCX. This was associated with decreased ICMS thresholds and, to a much smaller extent, enhanced somatic sensory responses in the

Address for reprint requests and other correspondence: J. H. Martin, Dept. of Physiology, Pharmacology and Neuroscience, City College of the City Univ. of New York, 160 Convent Ave., New York, NY 10031 (e-mail: jmartin@ccny.cuny.edu).

MCX, suggesting that motor more than sensory circuits were modulated by c-tsDCS. We also found that cervical spinal stimulation produced a larger effect on the forelimb than hindlimb and vibrissal motor maps, suggesting that the effect of c-tsDCS is preferentially mediated by cervical segmental circuits. Providing further qualitative explanation of the electrophysiological results, the FEM model showed maximal current density in the caudal cervical spinal cord for the electrode configuration we used. Our findings provide important new information that tsDCS is spatially selective and may improve voluntary motor function through MCX representational plasticity.

METHODS

A total of 17 adult female Sprague-Dawley rats (220~280 g) were used in this study, which included 1 rat for MRI and microcomputed tomography (micro-CT) scanning for the current density model, 5 rats for spinal reflex experiments, and 3 rats for breathing and heart rate experiments. Care and treatment of the animals conformed with protocols approved by the Institutional Animal Care and Use Committee of the City College of New York.

c-tsDCS. Electrodes for DC stimulation were modified by cutting two surface electrodes (StimTent Com) into a rectangular shape (15 × 20 mm). After the hair over the dorsal neck and chest of the animal was removed, electrical conductive adhesive was sprayed over the surface of electrodes, which helped stabilize effective electrical conduction between the skin and electrodes during the experiment. One electrode was placed over the C4-T2 vertebrae and the other pole was placed over the chest (see Fig. 1*B*). Cathodal stimulation refers to connecting negative current output to the dorsal C4-T2 surface electrode and positive current output to the chest electrode, whereas anodal stimulation refers to the opposite set of connections. We focused on cathodal stimulation for most of our experiments because cathodal, not anodal, stimulation augments spinal excitability as assayed by the H-reflex (see Fig. 3) and in preliminary experiments (Song and Martin 2013) only this polarity produced consistent effects on the cortically evoked motor responses [movements and motor evoked potentials (MEPs)]. tsDCS stimulation (± 3mA) was delivered through an analog isolated stimulator (model 2100, A-M Systems), which was controlled by a personal computer via an analog output card (USB 6009, National Instruments). The control program was developed with LabView (National Instruments).

tsDCS affects breathing in humans but does not affect other autonomic functions (Neriat et al. 2014). To control for possible autonomic and breathing effects in the rat with our stimulation, we determined if tsDCS across the dorsal neck and chest produced changes in heart rate and breathing rate. Heart rate was determined from the recorded ECG, which was recorded using percutaneous skin electrodes (right hindlimb and chest, close to the heart). Breathing was monitored using a force transducer coupled to abdominal skin. Both the ECG and signals from the force transducer were filtered (1-1,000 Hz) and acquired at a sampling frequency of 5 kHz. Rats ($n = 3$) were tested under three conditions: without tsDCS, with c-tsDCS, and with anodal tsDCS. We found no significant differences in either measure (heart rate: control 359 ± 9 beats/min, cathodal 359 ± 11 beats/min, and anodal 359 ± 11 beats/min, $P > 0.05$ by one-way ANOVA; and breathing rate: control 78 ± 2 breaths/min, cathodal 80 ± 2 breaths/min, and anodal 80 ± 3 breaths/min, $P > 0.05$ by one-way ANOVA).

ICMS mapping. Anesthesia was induced with a mixture of ketamine (80 mg/kg) and xylazine (5 mg/kg). The animal was placed in a stereotaxic frame (Kopf Instruments), and a craniotomy was made ~4.5 mm rostral and 2.5 mm caudal to the bregma and 1.5–6.5 mm lateral to the midline. This craniotomy completely exposed the forelimb and vibrissal MCX map as well as most of the hindlimb area (Starkey et al. 2012). The anesthesia level was checked by monitoring the breathing rate, vibrissae whisking, and hindlimb withdrawal to foot pinch. Supplemental doses of ketamine (25 mg/kg) were administered to maintain the required anesthetic depth during the experiment. A cerebrospinal fluid (CSF) drain was placed in the cisterna magna to reduce swelling. The dura of the MCX was removed, and silicone oil was applied over the cortex to prevent desiccation. Rats were maintained in a prone position within the stereotaxic frame. During the entire procedure, body temperature was maintained with a heating pad (39 ± 1°C) placed under the rat. A cotton swab was placed under the forearm to prop it up for easy observation of limb movements from a stable initial position. We mapped the MCX every 0.5 mm, between 1.5 and 4.5 mm medial-lateral and −1.5 to 4.5 mm rostral-caudal (relative to the bregma) at a depth of 1.5 mm from the dura. Unipolar parylene-coated tungsten sharp microelectrodes (tip diameter: 1–2 μm, 0.1–0.5 MΩ, Microprobes) were used for ICMS mapping. Constant current trains of 13 biphasic pulses (cathodal leading, with 200-μs duration at 300 Hz) were delivered at 1 Hz via an isolated stimulator (model 2100, A-M Systems). We tested for movement threshold at each site using a maximal current of 100 μA. The stimulation intensity was started at 40 μA. If a movement was evoked at this intensity, we decreased until no movement was observed; otherwise, we increased the intensity until a stable movement was induced and then decreased until no movement was observed. The movement threshold was defined as the minimum current at which a visible movement of any body part was evoked. For each site with a threshold of <80 μA, we further tested the threshold during c-tsDCS (−3 mA). If no movement was observed at 80 μA, we called this a nonresponsive site, and if no movement was observed at 100 μA, we did not test c-tsDCS at this site. To avoid potential aftereffects immediately after c-tsDCS, we waited at least 5 min before another testing, and this was further confirmed by retesting the threshold after c-tsDCS. Generally, we tested a site without c-tsDCS first and then with c-tsDCS, which could decrease the testing duration of c-tsDCS (maximum duration of 20 s). In preliminary experiments, we also tested c-tsDCS first (i.e., before the control condition), and no systematic changes were found. We therefore completed the control condition first for convenience. To avoid the possibility of a previous test affecting neighboring sites, we also counterbalanced the testing sites by penetrating one site locating in the middle and another at the edge of the mapping area.

H-reflex testing. To determine the effect of tsDCS on spinal reflex function in the rat, we used the H-reflex, similar to our previous study (Tan et al. 2012). We tested the reflex in two ways: *1*) stimulation of the isolated deep radial nerve and recording from extensor carpi radialis (ECR) muscle ($n = 3$ rats) or *2*) stimulating ECR muscle and recording from the interosseous muscle between the fourth and fifth digit of the forepaw ($n = 2$ rats). The more distal interosseous muscle recording allows for better separation of the M and H waves, which can be partially overlapping for the rat forelimb (Tan et al. 2012). Nevertheless, M and H waves were well separated in ECR recordings so we combined the results, normalized to control conditions. We examined the effects of both cathodal and anodal stimulation.

For nerve stimulation, the deep radial nerve was bluntly dissected to ensure minimal muscle damage and mounted within a bipolar cuff stimulating electrode. Teflon-insulated bipolar electromyograph electrodes (7 strained stainless steel, A-M Systems) with exposed tips (1 mm) were inserted 2 mm apart into the ECR muscle. Electromyographic responses to stimulation were filtered (0.1 Hz–10 kHz), amplified (×1,000), and sampled at frequency of 40 kHz (OmniPlex, Plexon). Responses were evoked with biphasic stimulating pulses (0.2 ms each phase, 10 responses/test) delivered every 3 s to determine the threshold of the M-wave response (T). Throughout all experiments, between 1.4T and 1.8T stimulation intensity provided the most consistent M and H wave responses. M and H wave amplitudes were quantified after rectifying and averaging the waveforms, and they were then normalized to the control condition (without DC) for each

rat. One-way ANOVA was applied for the group test and followed by post hoc testing for multiple comparisons with the Bonferroni correction.

Neural recording and sensory mapping. A 2 × 16 stainless steel microwire electrode array (wire diameter: 50 μm, interrow distance: 1.5 mm, intercolumn distance: 0.3 mm, TDT technology) was inserted in the sensorimotor cortex at depth of ~0.8 mm (layer IV). A ground wire was connected to a screw, which was secured to the occipital bone. A unity gain head stage was connected via flexible cables to the electrode array. Local field potentials (LFPs) were amplified (×1,000), low-pass filtered (0.1–300 Hz), and digitized at a sampling frequency of 1 kHz with OmniPlex-D (Plexon). Finally, LFPs were notch filtered to remove 60-Hz noise (notch, Matlab). SEPs are thought to represent initial afferent input arising from the postsynaptic responses of pyramid neurons (Pfurtscheller and Lopes da Silva 1999). SEPs from each electrode of the array were recorded from LFP responses to electrical stimulation of the contralateral (to MCX) wrist (subcutaneous bipolar electrode, with one on the dorsal skin surface and the other under the ventral skin surface). Sixty biphasic pulses (intensity: 0.5 mA, duration: 0.5 ms, frequency: 0.5 Hz) were delivered during each session (see the example in Fig. 5*A*). This stimulation could induce SEPs without noticeable muscle contractions, although activation of afferents other than cutaneous could not be ruled out. We classified recordings from each electrode as either responsive or nonresponsive to the electrical sensory stimulation from a SEP. A SEP-responsive site was defined as one in which the amplitude of the SEP within the response time window (poststimulus 10 to 25 ms for LFP) was >3 SD of baseline activity, which corresponded to the 20 ms preceding the stimulus. Thus, a limited sensory receptive filed map corresponding to the 2 × 16 recording array was constructed based on the amplitude of the SEP from the responsive sites.

The effect of c-tsDCS on ongoing LFP oscillations (as opposed to the evoked SEP) was analyzed using the event-related spectrum perturbation (ERSP) method, which is thought to reflect interactions between neurons and interneurons within the local cortical circuit (Pfurtscheller and Lopes da Silva 1999). The ERSP was calculated as a time-frequency representation with the wavelet method after removing the SEP from each trial and was then normalized to baseline at each power frequency band (Makeig 1993). As the low-frequency band (α/β; 8–30 Hz) presented a longer latency response than the high-frequency band (γl 30–70 Hz), we chose a response window for the α/β-band from 150 to 350 ms, whereas the window for the γ-band was from 0 to 50 ms after wrist stimulus onset (for examples, see Fig. 5, *C* and *D*). Similar to the above SEP analysis, for each recording electrode in the array, if the mean ERSP within the response window (see Fig. 5, *C* and *D*) was above 3 SD of its baseline activity (also 20 ms before the stimulus onset, for each frequency band), we called it an ERSP-responsive site. Finally, the mean spectrum powers of α/β- and γ-bands within their corresponding time-frequency response windows were used for the analysis.

FEM computational model to predict spinal regional current density during c-tsDCS. FEM computational models of tissue current flow during electrical stimulation, based on anatomic scans (MRI and CT), are considered reliable predictors of electric field and current density across the brain and spinal cord (Hernandez-Labrado et al. 2011; Rahman et al. 2013; Toshev et al. 2014). As the model makes only basic assumptions on physics (i.e., Ohms law), the precision of model predictions is limited by the quality of tissue segmentation and assigned tissue conductivity (Toshev et al. 2014). There have not been any published FEM current density models of the rat spinal cord; therefore, we constructed our own. We used MRI (7.0 Tesla 70/30 Bruker Biospec) with a TurboRARE T2-weighted pulse sequence to image soft tissues and micro-CT (Siemens Inveon) to image bone in one female rat. MRI settings achieved a 0.282-mm resolution and micro-CT achieved a 0.2-mm resolution. MRI and CT images were coregistered to the CT image space using functions available in Statistical Parametric Mapping (SPM8, Wellcome Trust Centre for Neuroimaging, London, UK). Segmentation was completed semimanually within ScanIP (Simpleware, Exeter, UK) with the aid of tools such as thresholding, threshold flood filling, Gaussian smoothing, dilation, and erosion. In each slice, the MR image of the brain and spinal cord was carefully outlined. The dura was traced, and the intervening space between the dura and brain or spinal cord comprised the CSF compartment. All soft tissues (including skin, muscle, fat, and tendons) comprised a single compartment. All bones were outlined from CT data.

The +Fe module of ScanIP was then used to generate an adaptive volumetric mesh of ~6.8 million tetrahedral elements. Electrostatic physics were modeled in COMSOL (COMSOL, Burlington, MA) using the following boundary conditions: inward current density summing to 3 mA on the ventral surface anode electrode, ground on the dorsal surface cathode electrode, insulation on all other external surfaces, and continuity for internal boundaries. Tissue conductivity for the model was assigned based on approximation from published values used in human simulation studies, which themselves are aggregates of animal data (Rahman et al. 2013; Toshev et al. 2014). We used the following values: soft tissue, 0.465 S/m; bone, 0.01 S/m; CSF, 1.65 S/m; gray matter, 0.276 S/m; white matter, 0.126 S/m; air, $1e^{-15}$ S/m; conductive gel or saline, 1.65 S/m; and electrode, $5.99e^{7}$ S/m. The electrode position was accurately referenced to the dorsal spinous process at T1 or the posterior ridge of the occipital bone and sternum, ventrally. The resulting finite element problem was solved for voltage and calculated current density. Results are presented both as current density on the reconstructed brain and spinal cord surfaces and within the spinal cord along the midsagittal axis.

Statistical analysis. We accessed differences between the control condition (without DC stimulation) and during the c-tsDCS condition by parametric (*t*-test, MATLAB) and nonparametric (ranksum or signrank, MATLAB) tests for data sets with a normal and non-normal distribution, respectively. The Bonferoni correction to *P* values was used for multiple comparisons. A Kolmogorov-Smirnov test was used to access the difference of distribution between two populations (kstest2, MATLAB). The significance level was set at 0.05 unless stated otherwise. All data analyses were performed using MATLAB (The Math Works).

RESULTS

FEM model of local current density. High-resolution micro-CT and MRI were performed, and bone, central nervous system (CNS), dura, and soft tissue were segmented to create separate anatomica compartments, each assigned a conductivity value. Magnetic resonance images of brain, spinal cord, and body soft tissues were coregistered with micro-CT imaging of bone in relation to the locations of the electrodes. Reconstructed images of the skeleton (Fig. 1*A*) and CNS within the dural sac and skeleton (Fig. 1*B*) showed typical rat anatomy. These results demonstrate the high anatomic resolution we achieved with the coregistered combined imaging. One cathode-anode (blue and pink, respectively; Fig. 1*B*) configuration is shown, which corresponds to the optimal placements (see below). We modeled several electrode configurations using the standard electrode size and a smaller electrode (25% of standard area) to estimate the local spinal and brain current density. Figure 2 shows the results for three key configurations, all with the standard electrode size. Figure 2, *A*, *C*, *E*, and *G*, shows surface views of the brain and spinal cord; Fig. 2, *B*, *D*, *F*, and *H*, shows slices through the midline, both according to the same color scale (*A*, *inset*). For Fig. 2, *A* and *B*, the highest current density is in the caudal cervical spinal cord, localized to the middle of the C5 to rostral T1 levels (*B*;

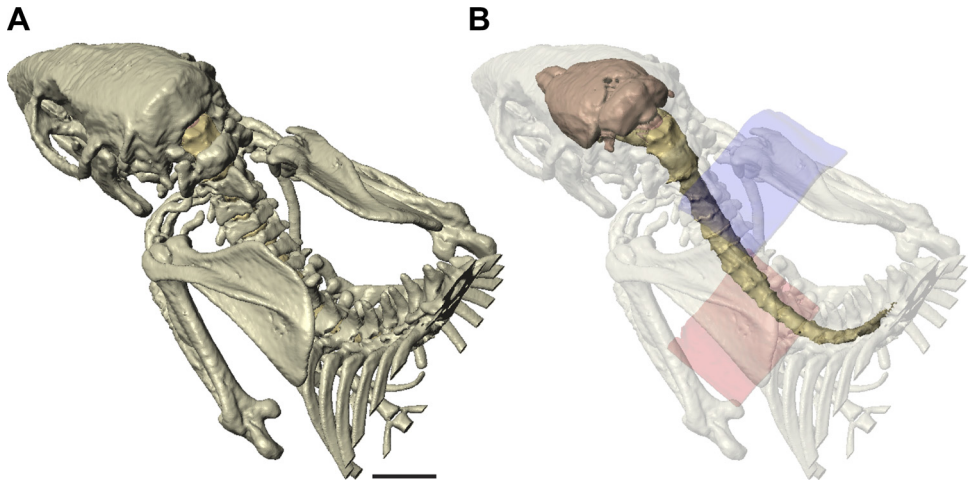

Fig. 1. High-resolution radiological imaging of the rat and tissue segmentation. *A*: rendering of bones imaged and segmented for the model. *B*: rendering of the brain and spinal cord within translucent bone. The cathode (blue, dorsal) and anode (pink, ventral) are shown. Length calibration: 10 mm for *A* and *B*.

arrow points to T1). There was proportionately smaller amounts of current at intervertebral spaces caudally and the foramen magnum (Fig. 2*B*) rostrally. The surface view also shows that the spinal roots are foci of higher current density. With a more rostral anode (Fig. 2, *C* and *D*), there was both a reduction in cervical enlargement current density and an increase in brain stem/cerebellar density. Finally, by shifting both electrodes rostrally (Fig. 2, *E* and *F*), the caudal cervical spinal cord was in the path of much less current. In contrast, there was a very high current density within the forebrain and brain stem. These results show that the more caudal electrode configuration (Fig. 2, *A* and *B*) is optimal because of the localization of higher current density to the caudal cervical enlargement. We therefore chose this electrode configuration for the physiological experiments. To better determine the current density within the spinal cord (i.e., gray matter) and the region of the spinal roots, we generated transverse images at selected rostrocaudal intervals for the optimal electrode configuration (Fig. 2, *G* and *H*). The most rostral segment (Fig. 2*H*) was through the intervertebral foramen/space, where the roots are located. The *inset* in Fig. 2*H* shows a schematic drawing of a spinal cord and associated roots. This shows the high current density in the region of the root and that the current density within the spinal cord is ~85% of the density near the root.

Effects of tsDCS on the forelimb H-reflex. Our preliminary experiments in the rat (Song and Martin 2013), as well as a study in the mouse (Ahmed 2011), indicated that c-tsDCS, not anodal tsDCS, effectively augmented corical-evoked responses (MEPs). To further justify use of cathodal stimulation and to inform the mechanisms of action of tsDCS, we examined the effect of anodal tsDCS and c-tsDCS on the amplitude of the H-reflex. In a representative example based on deep radial nerve stimulation and ECR recording, we show that cathodal stimulation augmented the H-reflex and anodal stimulation suppressed the reflex (Fig. 3*A*). Neither current changed the direct M response. Across the population, we normalized the responses during tsDCS to the nonstimulated control condition. There was no significant effect on the M response (control/no stimulation: 1, anodal tsDCS: 1.01 ± 0.01, and c-tsDCS: 1.02 ± 0.01, $P > 0.05$ by ANOVA). When we compared the effects of tsDCS on the H-reflex, we found that there were polarity-dependent changes, with reflex enhancement during c-tsDCS and suppression during anodal stimulation (Fig. 3*B*). The normalized H-to-M ratio also showed the same polarity-dependent changes as we saw for the H-reflex alone (Fig. 3*C*). The absence of an effect on the M wave suggests that neither polarity has a peripheral action, such as at the distal nerve or the muscle directly. The presence of facilitation with c-tsDCS supports results from a study in the human (Winkler et al. 2010) and provide further justification for using cathodal stimulation to enhance cervical spinal excitability to modify the MCX motor map.

Effects of c-tsDCS on the forelimb motor map. We used ICMS to probe the effect of cervical c-tsDCS on movement representation in the MCX. We first present data for the forelimb map, which we intended to modify with cervical c-tsDCS, and then complementary data for the hindlimb and vibrissal maps. We found that the current thresholds for evoking movement decreased (Fig. 4, *A* and *B*, shown as larger circles) and number of forelimb responsive sites increased during c-tsDCS compared with the control condition without tsDCS (Fig. 4, *A* and *B*; increased numbers of responsive sites, marked as colored and black dots). Overall, there was approximately a 20% increase in the size of the forelimb motor map, as assayed by the number of responsive sites (Fig. 4*C*). Consistent with prior observations (Ahmed 2011), MEPs recorded from the ECR in response to MCX stimulation were facilitated during c-tsDCS (Fig. 4*D*). In the representative experiments shown in Fig. 4, *A* and *B*, we stimulated a wrist site in the MCX (Fig. 4, *A* and *B*, arrows) both during the control condition without c-tsDCS and with c-tsDCS and observed an increase in the peak to peak amplitude of the MEP when c-tsDCS was applied (Fig. 4*D*,*1*). Interestingly, we observed a comparable enhancement in the MEP amplitude when an epidural electrode was used, which activated a large region of the MCX (Fig. 4*D*, *2*).

Since a larger response was consistently evoked during c-tsDCS, we analyzed threshold changes at all sites. We compared the threshold for evoking a forelimb response under control and c-tsDCS conditions and found a significant reduction ($P < 0.05$ by *t*-test; Fig. 4*E*). Note that there were sites that were not effective in producing a motor response under the control condition but were effective during c-tsDCS. These sites were not included in this comparative analysis but nonetheless support the finding of increased efficacy of evoking a movement with cervical c-tsDCS.

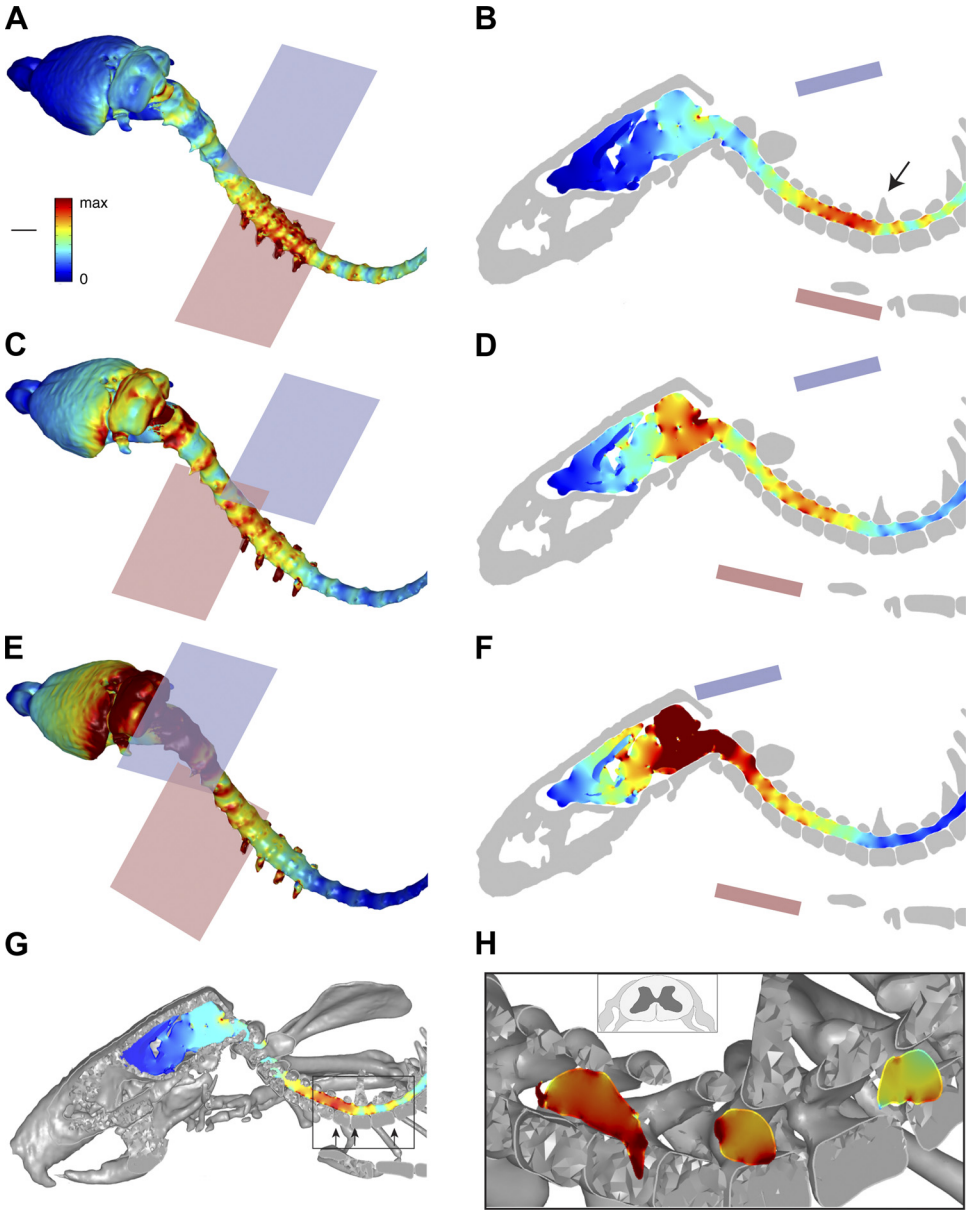

Fig. 2. Finite-element method (FEM) modeling to predict regional current density. Surface views (*A*, *C*, and *E*) and midsagittal slices (*B*, *D*, and *F*) through the brain and spinal cord showing regional current density. The locations of the cathode (blue, dorsal) and anode (pink, ventral) are shown in each image. *A* and *B*: the cathode was positioned in relation to the T1 spinous process (arrow, *B*) and the anode was positioned in relation to the sternum. *C* and *D*: the anode was displaced rostrally relative to the position shown in *A* and *B*. *E* and *F*: both the cathode and anode were displaced rostrally in relation to the positions in *A* and *B*. *G* and *H*: intraspinal and spinal root current density. *G*: oblique view of the vertebrae and central nervous system close to the midline. Some of the rostral spinal cord segments are partially obscured by bony structures. Arrows within the boxed area point to the enlarged image and the location of three transverse spinal images in *G*. *H*: transverse images at selected cervical intervertebral levels. Note that the most rostral transverse image (*H*, left arrow) shows the left root. The *inset* in *H* shows a schematic of a spinal cord segment and associated dorsal and ventral roots. Current density calibration: 1.14 A/m^2. Length: 8.26 mm.

Differential effects of cervical c-tsDCS on forelimb, hindlimb, and vibrissal motor representations. We next determined if cervical c-tsDCS had a preferential effect on the forelimb motor map or if similar effects were produced for the hindlimb and vibrissal maps. Compared with the forelimb, there were substantially smaller increases in hindlimb and vibrissal motor maps (Fig. 4, *A*–*C*). There was a small significant reduction in the hindlimb movement threshold ($P < 0.05$ by *t*-test) and no significant change in vibrissae movement thresholds (Fig. 4*E*).

To determine the differential effects of cervical c-tsDCS on the population of M1 sites examined, we plotted the cumulative threshold change for all sites in all animals (Fig. 4*F*). The cumulative threshold distribution for the forelimb (red arrow, 20% shift) was significantly greater than both hindlimb (green arrow) and vibrissal (blue arrow) representations ($P < 0.05$ for each pair-wise comparison by kstest). The *inset* in Fig. 4*F* shows a plot of the mean threshold reduction. There was a significant threshold reduction for the forelimb compared with hindlimb and vibrissal representations ($P < 0.05$ by *t*-test after Bonferoni correction). These findings show that cervical c-tsDCS produced a significant and preferential enlargement of the forelimb motor map and that this was associated with a larger reduction in the forelimb motor threshold that either the hindlimb or vibrissae.

Effects of c-tsDCS on the somatic sensory map in the MCX. c-tsDCS can influence somatic sensory processing (Aguilar et al. 2011), and this could, in turn, affect the MCX motor map (Jiang et al. 2013) and the efficacy of MCX stimulation. We next examined the effect of cervical c-tsDCS on somatic sensory representation in the MCX. We placed percutaneous electrodes at the wrist contralateral to the microelectrode array, which was positioned over the forelimb area of M1 after the motor mapping (ICMS) was complete. The array comprised two rows of microelectrodes, oriented parallel to the midline. We recorded the initial evoked somatic sensory response to wrist cutaneous stimulation, termed the SEP (10–25 ms after the stimulus onset). Electrical stimulation at the wrist reliably

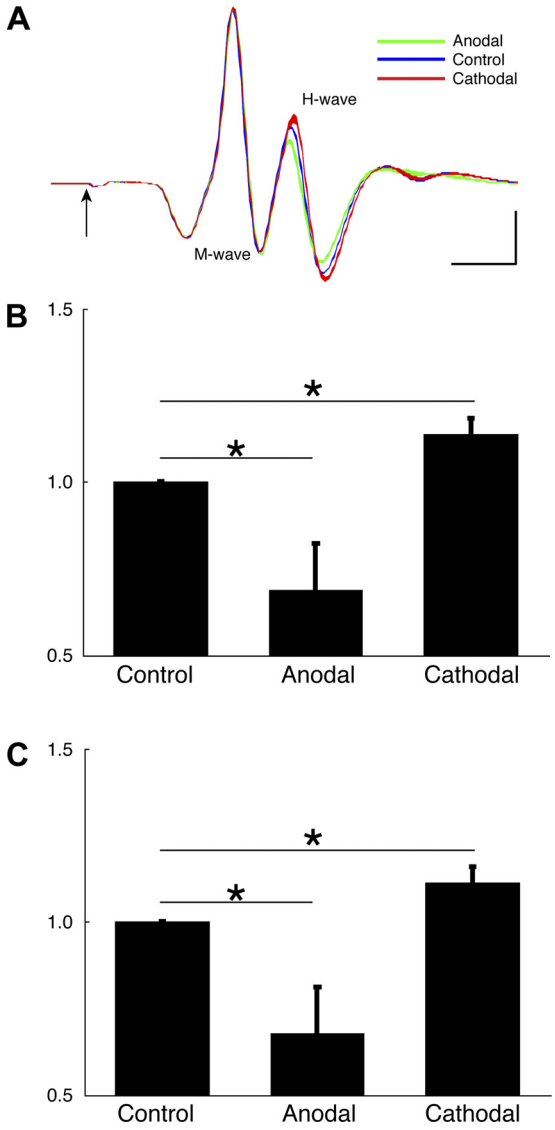

Fig. 3. Effects of anodal tsDCS and c-tsDCS on the H-reflex. *A*: example of an M wave and H wave recorded from the extensor carpi radialis (ECR) muscle when stimulating the deep radial nerve. Color band represents 95% confidence interval (average of 10 stimuli). The arrow marks the stimulus onset (artifact blanked). Calibration: 1 ms, 5 mV. *B* and *C*: the H wave (*B*) and H-to-M ratio (*C*) were normalized to the control amplitude condition to correct for between-animal differences. For both *B* and *C*, anodal tsDCS produced a significant decrease and c-tsDCS showed a significant increase in the normalized H wave and H-to-M ratio. Values are means ± SE; $n = 5$ animals. *$P < 0.05$ by one-way ANOVA followed by post hoc pairwise comparison with the Bonferoni correction.

induced SEPs both during the control condition and with c-tsDCS, as shown in a representative experiment (Fig. 5, *A* and *B*). Overall, we found a close correspondence between wrist motor and wrist sensory sites. Whereas wrist sensory responses were commonly evoked at elbow and shoulder zones, they were not commonly recorded at vibrissae zones. Mean SEP amplitude for each recording site was plotted in relation to electrode location. The peak to peak SEP amplitude was plotted as a color scale to construct the maps shown in Fig. 5, *A* and *B*. For comparison, sites where ICMS evoked wrist movement were overlaid, aligned closely with the electrode positions. Whereas a few sites were not responsive to wrist peripheral stimulation (blue), most showed moderate- to large-amplitude responses under both control and c-tsDCS conditions.

We quantified changes produced by c-tsDCS at each recording site in the array. Responsive SEP sites were defined as a SEP that was >3 SD of the baseline. Under the c-tsDCS condition, there was a small increase in the number of responsive sites ($n = 165$ sites without c-tsDCS and 174 sites with c-tsDCS; Fig. 6*A*, white and blue bars). Some sites were only responsive under the control condition ($n = 5$), and a few sites were recruited only during c-tsDCS ($n = 14$). For the major class of site in which SEPs were responsive both without and with c-tsDCS, we calculated the SEP amplitude percent change between the control and c-tsDCS conditions. We plotted the percent change as a cumulative distribution for all sites (Fig. 6*B*, blue). There was a small rightward shift. Comparison of absolute SEP values at each of these sites, without and with c-tsDCS, revealed a 13% increase (Fig. 6*C*), which was significant ($P < 0.05$ by *t*-test). This shows that c-tsDCS produced a small significant increase in the SEP to wrist sensory stimulation.

Sensory stimulation not only directly evoked a SEP but also induced cortical oscillations in different frequency bands and at different latencies; this is termed the ERSP, which is thought to reflect the interaction between neurons within the local cortical circuit (Pfurtscheller and Lopes da Silva 1999). The ERSP demonstrates a network response to stimulation that, if modulated by c-tsDCS, could help inform how c-tsDCS affects the motor map. The ERSP to wrist stimulation is shown as a two-dimensional time-frequency heatmap (Fig. 5, *C* and *D*) with color representing the amplitude of the response. We choose two windows of interest, which showed consistent time-frequency representation in the high-frequency and low-frequency bands under control conditions (Fig. 5*C*), to characterize the frequency response across sessions and animals. The high-frequency power showed an early response during the control/no c-tsDCS condition (see boxed region labeled γ), and the low-frequency power showed a late response (boxed region labeled α/β).

c-tsDCS modulated the somatic sensory network response as shown in ERSP map (Fig. 5*D*). Similar to the analysis of SEP, we also classified ERSP-responsive sites and quantified the percent changes during c-tsDCS in the separate γ- and α/β-band windows (boxes) at each recording site. There was a small increase in ERSP-responsive sites under the c-tsDCS condition for the α/β-band ($n = 94$ sites without c-tsDCS and 104 sites with c-tsDCS; Fig. 6*A*, white and green bars) and no change for the γ-band ($n = 100$ sites without c-tsDCS and 98 sites with c-tsDCS; Fig. 6*A*, white and brown bars). For sites in which an ERSP was responsive both without and with c-tsDCS, we determined the amplitude percent change between the control and c-tsDCS conditions, similar to the SEP. The cumulative distribution of percent change showed a small significant ($P < 0.05$ by paired *t*-test) rightward shift in the α/β frequency range (9.5%) and no significant shift for the γ frequency range (−0.2%). Overall, our findings show that c-tsDCS augmented, albeit modestly, wrist sensory processing in the MCX.

Comparison of effects of c-tsDCS on motor and sensory responses. To compare the effect of c-tsDCS on the forelimb

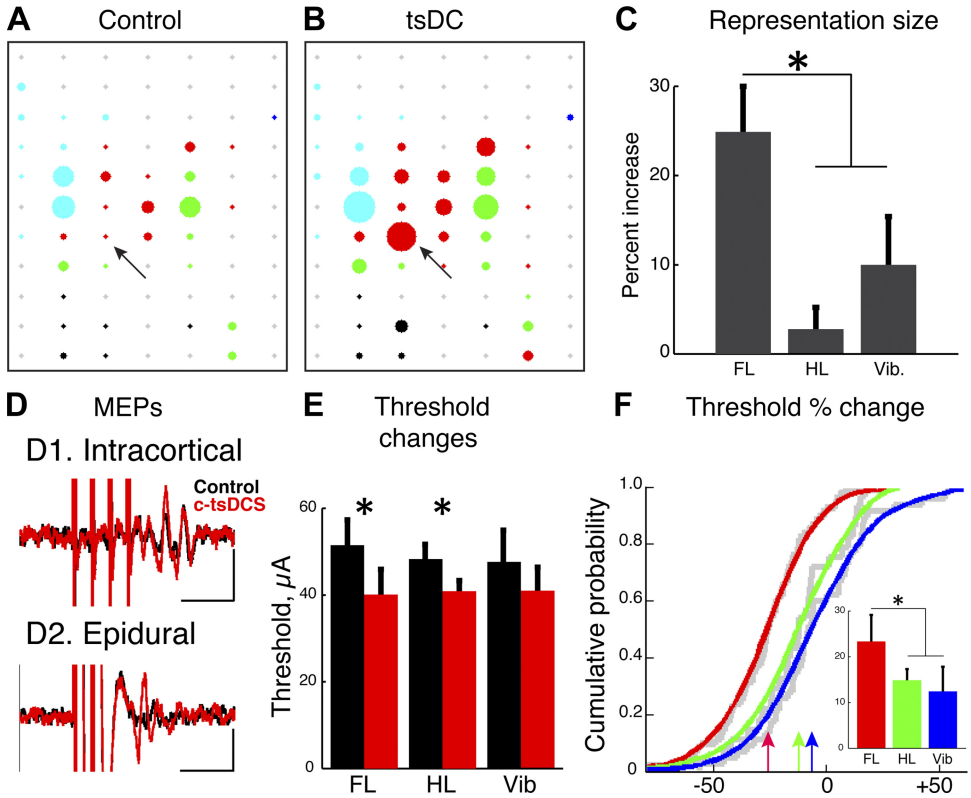

Fig. 4. Effect of c-tsDCS on the motor cortex (MCX) motor representation. *A* and *B*: representative motor maps plotting the threshold of intracortical microstimulation (ICMS) as a circle in which the diameter is inversely proportional to the threshold during the control condition (*A*) and during c-tsDCS (*B*). Red, wrist; green, elbow; blue, shoulder; black, hindlimb; cyan, whisker; gray, nonresponsive sites. Arrows point to site from which motor evoked potentials (MEPs) were evoked from ECR muscle when stimulating the MCX in D1. *C*: c-tsDCS produced a differential expansion of forelimb (FL), hindlimb (HL), and vibrissal (Vib) sites. The percent increase was the largest for the forelimb area than both hindlimb and vibrissal areas ($P < 0.05$ by paired *t*-test). *D*: the decrease in ICMS threshold was accompanied by an increase in the amplitude of MEPs for a given stimulus intensity recorded from forelimb muscles when tested with either a sharp electrode (D1: depth at 1.5 mm, intensity: 0.2 mA, 4 pulses of 200-μs duration at 300 Hz) or an epidural electrode (D2: PlasticOne electrode, intensity: 3 mA, 4 pulses of 200-μs duration at 300 Hz). Calibration: 10 ms, 5 mV. *E*: c-tsDCS produced significant reductions in mean ICMS threshold for sites in forelimb and hindlimb areas compared with control ($P < 0.05$ by paired *t*-test) but not the vibrissal area. *F*: cumulative distribution histograms plotted for all stimulation sites. The threshold reduction produced during c-tsDCS was significantly greater for the forelimb than that of either the hindlimb area or whisker (Vib) area (pairwise comparisons, $P < 0.05$ by *t*-test and kstest2), whereas there was no significant difference between hindlimb and whisker areas. The *inset* shows the mean percent threshold reduction during c-tsDCS (*$P < 0.05$ by *t*-test). The colored lines in *F* represent the theoretical distributions of the underlying empirical cumulative distribution functions (gray lines).

motor and sensory responses, we chose the unitless percent change (responses normalized to control condition). We replotted the percent decrease in motor threshold (Fig. 4*F*) as an increase to facilitate comparison with the increased sensory response (Fig. 6*B*) during c-tsDCS stimulation. The motor threshold percent reduction (rightward shift) was larger than the percent increases in either SEP or ERSP ($P < 0.05$ for each comparison by kstest2). We further compared the changes in evoked MEP amplitude (ECR across all experiments; flexor carpi radialis, biceps, triceps, and shoulder less frequently) with sensory response changes. Pooling data across all forelimb MEP recordings ($n = 24$ sites, 7 rats), there was a 33.4 ± 5.6% increase in MEP amplitude during c-tsDCS, similar to what we observed for the percent threshold reduction (26.2 ± 2.4%). The MEP amplitude increase was significantly greater than changes observed for the sensory responses ($P < 0.05$ by ANOVA with Bonferoni multiple comparisons correction). These data suggest a significantly greater effect of c-tsDCS on the motor map, assayed both as a threshold reduction and MEP amplitude increase, than on the sensory map, assayed as an increase in response amplitude.

DISCUSSION

Cortical motor map reorganization is commonly observed after learning (Kleim et al. 1998, 2004), peripheral or CNS injury (Kaas 2000; Sanes et al. 1988), or induced artificially with long-term electrical stimulation or persistent conditioning based on spike timing-dependent plasticity (Ganguly et al. 2011; Jackson et al. 2006; Nishimura et al. 2013). We found that cervical c-tsDCS augments the cortical motor map, by threshold reduction and differential enlargement of the forelimb representation, during the brief stimulation period. Our findings point to the principal mechanism for this augmentation as increased cervical spinal circuit excitability. FEM modeling showed that the highest current density was localized to the caudal cervical enlargement. We found that c-tsDCS also enhanced the H-reflex, in contrast to anodal stimulation, which depresses the reflex, as in the human (Winkler et al. 2010).

A key question is what neural elements in the cervical spinal cord are mediating the direct effects of tsDCS? A recent modeling study (Danner et al. 2011) suggested that the dorsal roots had a lower threshold for activation by phasic epidural stimulation than dorsal column axons. Our model in the rat presents similar results in that local current density was great-

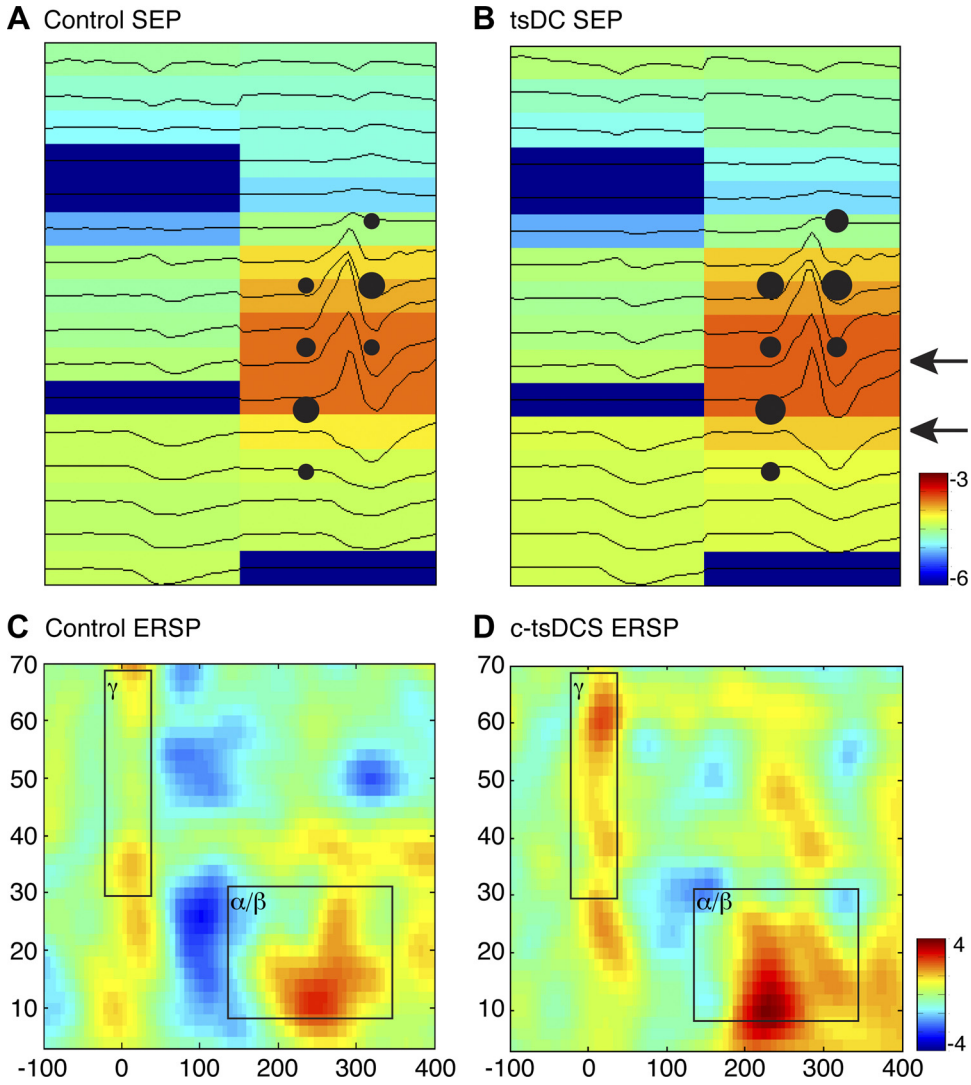

Fig. 5. Effect of c-tsDCS on somatic sensory representation in the MCX. *A* and *B*: representative somatic sensory maps are showing a broad cortical response to wrist cutaneous electrical stimulation during the control condition (*A*) and during c-tsDCS (*B*). The sensory evoked potentials (SEP) heatmap (log scale for visualization) was constructed from each recording site of a 2 × 16 microelectrode array using the peak amplitude of the SEP (black line) within a response window (10–25 ms from the stimulation onset). The dark blue sites and associated flat lines indicate nonresponsive sites. For the same experiment, sites where ICMS evoked a wrist movement were superimposed. Note the close correspondence of the two maps. *C* and *D*: representative event-related spectrum perturbations (ERSPs) during the control condition (*C*) and during c-tsDCS (*D*). Stimulation produced an early response in the high-frequency (γ) power range and a longer latency response in the low-frequency (α/β) power range (black squares). Powers at γ- and α/β-bands were averaged at each corresponding windows for the data shown in Fig. 3. Calibration: −6 to −3 dB in *A* and *B* and −4 to +4 dB in *C* and *D*.

est in the region of spinal roots. Interestingly, current density also was high intraspinally at the levels of the intervertebral spaces. This likely contributed to the high current density at the roots, which exit the cord through the intervertebral spaces. The intervertebral spaces are high-conductance paths for tsDCS. These findings suggest that the roots may be activated during tsDCS because current density is high. However, our findings also suggest that peripheral activation is weak, based on physiological responses, and that there also may be intraspinal activation because intraspinal current density is high. First, had tsDCS strongly activated the dorsal roots, we would have expected stronger augmentation of the sensory-evoked responses, but only modest effects were observed. Second, the amplitude of the M wave, the directly evoked muscle response, was not changed with c-tsDCS, suggesting that the increased H-reflex response during tsDCS arises more from within the spinal cord than the periphery. Third, consistent with central activation, intraspinal current density was nearly as high as at the roots. c-tsDCS has been shown to activate spinal central pattern generators (CPGs) in rodents (Ahmed 2013b). Intraspinal activation is akin to the direct effect of tDCS on local cortical circuits (Bikson et al. 2004; Rahman et al. 2013). Since the major effects of c-tsDCS were to reduce the forelimb motor thresholds and expand the forelimb motor representation, we propose that motor map enhancement occurred because pyramidal neurons projecting to the cervical spinal cord, either directly via the CST or indirectly via cortex to brain stem pathways, are better able to excite spinal motor circuits and evoke a motor response. To summarize, results of our FEM model, based on locally high current density, suggests that during the period of c-tsDCS, there was both increased intrinsic spinal circuit excitability and some root activation.

Spinal motor more than sensory circuits are the site of action for c-tsDCS. Is motor map augmentation due to facilitation of spinal motor circuits? The larger overall change in motor than somatic sensory responses (Fig. 6C) could be explained by direct activation of local spinal motor circuits by c-tsDCS, where last-order interneurons and motor neurons are located (Asante and Martin 2013; Baldissera et al. 1981). Importantly, c-tsDCS can activate spinal CPGs (Ahmed 2013b) and enhance H-reflex function, stressing a central motor circuit action. The larger H-reflex could have a presynaptic (e.g., stronger group 1A activation or reduced presynaptic inhibition) or postsynaptic (increased motoneuron excitability) locus. However, plasticity at the distal CST axon cannot be excluded as playing a role in forelimb map enhancement. As

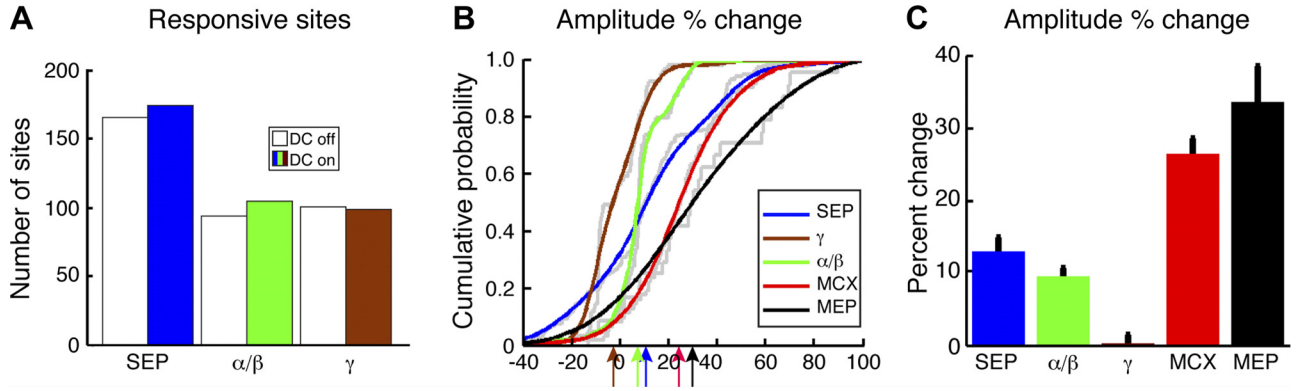

Fig. 6. Population sensory responses and comparison with motor responses. *A*: distribution of responsive sites (see definition in METHODS) during sensory stimulation for the entire population. Both SEP and ERSP power demonstrated responses to sensory stimulation during both control (no c-tsDCS) and c-tsDCS conditions. *B*: cumulative distribution histograms of response probability plotted based on the subpopulation of sites in which there was a significant response recorded during both control and c-tsDCS conditions. During the c-tsDCS condition, there was significant facilitation of SEP and ERSP in the α/β-band ($P < 0.05$ by paired *t*-test) but not in the γ-band. The percent change was significantly different between different signal sources ($P < 0.05$ by kstest2). SEP amplitude changes and changes in the α/β-band response of the ERSP were less than forelimb motor threshold changes during ICMS (red line replotted from Fig. 4*F* but reversed in sign to facilitate comparison) and the MEP amplitude increase. *C*: the effect of c-tsDCS on motor threshold change and MEP amplitude increase was significantly larger than either the changes in SEP or ERSP ($P < 0.05$ by *t*-test for each comparison).

much of the corticospinal output is mediated by spinal interneurons (Illert et al. 1976), induced activation of different spinal motor interneuronal circuits by c-tsDCS could be a powerful way to facilitate cortical motor functions.

c-tsDCS generated an electric field that had the highest density in the caudal cervical and rostral thoracic spinal cord, which will polarize the membrane of the underlying neurons and axons (Bikson et al. 2004; Rahman et al. 2013). The strong effect of c-tsDCS on the forelimb representation, weak effect on the hindlimb representation, and no significant effect on the whisker representation is consistent with the current maximally affecting motor circuits in the cervical enlargement. Although we cannot rule out a weak effect on passing CST fibers, long descending propriospinal networks originating from the cervical cord and projecting to the lumbar spinal cord (Bareyre et al. 2004; Reed et al. 2009) could mediate the weak modulatory effect on evoked hindleg motor responses that we observed. That vibrissal effects were not significant suggest that there was insufficient caudal brain stem current flow to affect the excitability of brain stem neurons, such as in the trigeminal or dorsal column nuclei. The model predicted increased current density in hindbrain structures near the foramen magnum and, because of this, we cannot rule out some brain stem and cerebellar activation by spinal c-tsDCS. Although we used FEM modeling to optimize electrode locations, an interesting next methodological step would be to use the model to predict quantitatively the physiological actions of other electrode configurations.

Since c-tsDCS also augmented MCX somatic sensory processing, albeit to a significantly lesser extent than for the motor threshold, cortical neurons may be more excitable and have a reduced threshold for activation by ICMS because of intracortical changes. tsDCS could also modulate the membrane potential of ascending spinal cord projection neurons to affect MCX somatic sensory processing. These actions of c-tsDCS on somatic sensory pathways would be mediated via an indirect long loop path to MCX. The MCX SEP is the postsynaptic response of pyramid neurons, whereas the ERSP reflects the complex feedforward and feedback interactions between MCX cortical neurons and local interneurons (Pfurtscheller and Lopes da Silva 1999). This long loop activation is consistent with recent findings showing that tsDCS over lumber spinal cord affects ascending signals (Aguilar et al. 2011; Ahmed 2013a, 2013b). It was further reported that changes in evoked responses in the primary somatic sensory cortex were variable during thoracic spinal DCS and dependent on brain state (Aguilar et al. 2011). We recorded from the MCX, which may receive somatic sensory input by even less direct subcortical projections than the somatic sensory cortex (Asanuma 1981). It was surprising that we observed consistent, albeit small, changes in the SEP. Recently, we have shown that the MCX motor map, especially the distal representation, depends on limb afferent input (Jiang et al. 2013). Together, these findings suggest that the ascending forelimb somatic sensory input pathway and descending corticospinal projection from forelimb sensorimotor cortex comprise a network that is modulated by c-tsDCS. The presence of a small influence on the SEP, the likely first stage in intracortical processing, and an even smaller effect on the ERSP further suggests that c-tsDCS modulation of somatic sensory processing is less important than its motor effects.

Translational potential of tsDCS to activate spinal motor circuits. Activation of spinal motor circuits holds much promise to improve motor function in humans after spinal cord injury (Edgerton et al. 2008; Edgerton and Roy 2012). For example, phasic epidural stimulation of the lumbosacral spinal cord was found to improve locomotion after spinal cord injury in humans (Harkema et al. 2011), and the effects of a similar phasic stimulation showed a frequency and segmental level dependency (Minassian et al. 2004). This phasic stimulation is thought to activate CPGs and sensory inputs (Gerasimenko et al. 2008). Similarly, evidence supports spinal cord activation in tsDCS, especially cathodal stimulation as shown in our study with H-reflex response enhancement and in the mouse (Ahmed 2011). tsDCS is just as well suited as phasic epidural spinal stimulation for motor rehabilitation/training. The noninvasive application of tsDCS using surface electrodes is appropriate for behaving animals (Song and Martin 2013) and humans.

FEM modeling shows that the physical characteristics of the DC stimulus, including current density and flow, can be pre-

dicted (Toshev et al. 2014), which enables more precise targeting of stimulation to particular neural regions, as we have done for the spinal cord. We hypothesize that tsDCS may activate diffusely the neural tissue experiencing the highest current density. This could be leveraged for two purposes. First, activity-dependent processes would generally be facilitated within the targeted regions. Second, selectivity of neural circuit activation might be achieved by concurrent weak phasic stimulation of spinal inputs and c-tsDCS. For example, muscle afferent stimulation, which can broadly activate spinal circuits at threshold (e.g., Edgley and Jankowska 1987), may selectively activate particular spinal regions that are stimulated at subthreshold levels along with c-tsDCS.

It is important also to consider that tsDCS would enable modulation of spinal circuit excitability without producing timing-dependent interactions with phasic stimulation of other sites (Bi and Poo 2001; Dan and Poo 2004). On the one hand, timing-dependent plasticity can be strongly facilitatory, so that tsDCS misses out on this opportunity. On the other hand, at nonoptimized interstimulus intervals, stimulus-dependent timing can be strongly suppressive. Thus, tsDCS could be implemented clinically without precise electrophysiological testing for optimal interstimulus intervals.

Whereas no electrical stimulation approach can be completely selective for a single neural circuit or function, we show here that cervical c-tsDCS preferentially facilitates the forelimb motor map, suggesting physiological actions primarily on the cervical spinal cord. The FEM model provides strong support for maximal current density within the cervical enlargement, which is the optimal location for affecting forelimb motor output. Importantly, our study is in a small animal model where the physical constraints are substantially different from the human. Electrode proximity to the spinal cord enables high intraspinal current density and clear physiological effects. However, in the rat, even small amounts of current spread could lead to the activation of hindleg circuits. We expect that tsDCS can be more selective in the human, albeit at lower current densities. With more complex electrode configuration design, further selectivity at high currents might be achieved in the human.

ACKNOWLEDGMENTS

The authors thank Dr. Henning Voss and the Citigroup Biomedical Imaging Center, Weill Cornell Medical College (New York, New York), for help with MRI and CT imaging. The authors also thank Malcolm Winkle for help with tissue segmentation.

GRANTS

This work was supported by National Institute of Neurological Disorders and Stroke Grant 2R01NS064004 (to J. H. Martin) and Craig H. Neilsen Foundation Grant 261214 (to J. H. Martin).

DISCLOSURES

The City University of New York has patents on brain stimulation with M. Bikson as inventor. M. Bikson has equity in Soterix Medical.

AUTHOR CONTRIBUTIONS

Author contributions: W.S., M.B., and J.H.M. conception and design of research; W.S. and D.Q.T. performed experiments; W.S. and D.Q.T. analyzed data; W.S., D.Q.T., M.B., and J.H.M. interpreted results of experiments; W.S., D.Q.T., and J.H.M. prepared figures; W.S. and J.H.M. drafted manuscript; W.S., M.B., and J.H.M. edited and revised manuscript; W.S., D.Q.T., M.B., and J.H.M. approved final version of manuscript.

REFERENCES

Aguilar J, Pulecchi F, Dilena R, Oliviero A, Priori A, Foffani G. Spinal direct current stimulation modulates the activity of gracile nucleus and primary somatosensory cortex in anaesthetized rats. *J Physiol* 589: 4981–4996, 2011.

Ahmed Z. Effects of cathodal trans-spinal direct current stimulation on mouse spinal network and complex multijoint movements. *J Neurosci* 33: 14949–14957, 2013a.

Ahmed Z. Electrophysiological characterization of spino-sciatic and cortico-sciatic associative plasticity: modulation by trans-spinal direct current and effects on recovery after spinal cord injury in mice. *J Neurosci* 33: 4935–4946, 2013b.

Ahmed Z. Trans-spinal direct current stimulation modulates motor cortex-induced muscle contraction in mice. *J Appl Physiol* 110: 1414–1424, 2011.

Alonzo A, Brassil J, Taylor JL, Martin D, Loo CK. Daily transcranial direct current stimulation (tDCS) leads to greater increases in cortical excitability than second daily transcranial direct current stimulation. *Brain Stimul* 5: 208–213, 2012.

Asante CO, Martin JH. Differential joint-specific corticospinal tract projections within the cervical enlargement. *PLos One* 8: e74454, 2013.

Asanuma H. Functional role of sensory inputs to the motor cortex. *Prog Neurobiol* 16: 241–262, 1981.

Baldissera F, Hultborn H, Illert M. Integration in spinal neuronal systems. In: *Handbook of Physiology. The Nervous System. Motor Control*. Bethesda, MD: Am. Physiol. Soc., 1981, sect. 1, vol. II, pt. 1, chapt. 12, p. 509–596.

Bareyre FM, Kerschensteiner M, Raineteau O, Mettenleiter TC, Weinmann O, Schwab ME. The injured spinal cord spontaneously forms a new intraspinal circuit in adult rats. *Nat Neurosci* 7: 269–277, 2004.

Bi G, Poo M. Synaptic modification by correlated activity: Hebb's postulate revisited. *Annu Rev Neurosci* 24: 139–166, 2001.

Bikson M, Inoue M, Akiyama H, Deans JK, Fox JE, Miyakawa H, Jefferys JG. Effects of uniform extracellular DC electric fields on excitability in rat hippocampal slices in vitro. *J Physiol* 557: 175–190, 2004.

Cambiaghi M, Velikova S, Gonzalez-Rosa JJ, Cursi M, Comi G, Leocani L. Brain transcranial direct current stimulation modulates motor excitability in mice. *Eur J Neurosci* 31: 704–709, 2010.

Dan Y, Poo MM. Spike timing-dependent plasticity of neural circuits. *Neuron* 44: 23–30, 2004.

Danner SM, Hofstoetter US, Ladenbauer J, Rattay F, Minassian K. Can the human lumbar posterior columns be stimulated by transcutaneous spinal cord stimulation? A modeling study. *Artif Organs* 35: 257–262, 2014.

da Silva MC, Conti CL, Klauss J, Alves LG, do Nascimento Cavalcante HM, Fregni F, Nitsche MA, Nakamura-Palacios EM. Behavioral effects of transcranial direct current stimulation (tDCS) induced dorsolateral prefrontal cortex plasticity in alcohol dependence. *J Physiol* 107: 493–502, 2013.

Edgerton VR, Courtine G, Gerasimenko YP, Lavrov I, Ichiyama RM, Fong AJ, Cai LL, Otoshi CK, Tillakaratne NJ, Burdick JW, Roy RR. Training locomotor networks. *Brain Res Rev* 57: 241–254, 2008.

Edgerton VR, Roy RR. A new age for rehabilitation. *Eur J Phys Rehabil Med* 48: 99–109, 2012.

Edgley SA, Jankowska E. Field potentials generated by group II muscle afferents in the middle lumbar segments of the cat spinal cord. *J Physiol* 385: 393–413, 1987.

Ganguly K, Dimitrov DF, Wallis JD, Carmena JM. Reversible large-scale modification of cortical networks during neuroprosthetic control. *Nat Neurosci* 14: 662–667, 2011.

Gerasimenko Y, Roy RR, Edgerton VR. Epidural stimulation: comparison of the spinal circuits that generate and control locomotion in rats, cats and humans. *Exp Neurol* 209: 417–425, 2008.

Harkema S, Gerasimenko Y, Hodes J, Burdick J, Angeli C, Chen Y, Ferreira C, Willhite A, Rejc E, Grossman RG, Edgerton VR. Effect of epidural stimulation of the lumbosacral spinal cord on voluntary movement, standing, and assisted stepping after motor complete paraplegia: a case study. *Lancet* 377: 1938–1947, 2011.

Hernandez-Labrado GR, Polo JL, Lopez-Dolado E, Collazos-Castro JE. Spinal cord direct current stimulation: finite element analysis of the electric field and current density. *Med Biol Eng Comput* 49: 417–429, 2011.

Illert M, Lundberg A, Tanaka R. Integration in descending motor pathways controlling the forelimb in the cat. 2. Convergence on neurones mediating disynaptic cortico-motoneuronal excitation. *Exp Brain Res* 26: 521–540, 1976.

Jackson A, Mavoori J, Fetz EE. Long-term motor cortex plasticity induced by an electronic neural implant. *Nature* 444: 56–60, 2006.

Javadi AH, Cheng P, Walsh V. Short duration transcranial direct current stimulation (tDCS) modulates verbal memory. *Brain Stimul* 5: 468–474, 2012.

Jiang YQ, Williams PT, Martin JH. Rapid and persistent impairments of the forelimb motor representations following cervical deafferentation in rats. *Eur J Neurosci* 38: 3702–3711, 2013.

Kaas JH. The reorganization of somatosensory and motor cortex after peripheral nerve or spinal cord injury in primates. *Prog Brain Res* 128: 173–179, 2000.

Kleim JA, Barbay S, Nudo RJ. Functional reorganization of the rat motor cortex following motor skill learning. *J Neurophysiol* 80: 3321–3325, 1998.

Kleim JA, Hogg TM, VandenBerg PM, Cooper NR, Bruneau R, Remple M. Cortical synaptogenesis and motor map reorganization occur during late, but not early, phase of motor skill learning. *J Neurosci* 24: 628–633, 2004.

Makeig S. Auditory event-related dynamics of the EEG spectrum and effects of exposure to tones. *Electroencephalogr Clin Neurophysiol* 86: 283–293, 1993.

Minassian K, Jilge B, Rattay F, Pinter MM, Binder H, Gerstenbrand F, Dimitrijevic MR. Stepping-like movements in humans with complete spinal cord injury induced by epidural stimulation of the lumbar cord: electromyographic study of compound muscle action potentials. *Spinal Cord* 42: 401–416, 2004.

Monfils MH, Plautz EJ, Kleim JA. In search of the motor engram: motor map plasticity as a mechanism for encoding motor experience. *Neuroscientist* 11: 471–483, 2005.

Nierat MC, Similowski T, Lamy JC. Does trans-spinal direct current stimulation alter phrenic motoneurons and respiratory neuromechanical outputs in humans? A double-blind, sham-controlled, randomized, crossover study. *J Neurosci* 34: 14420–14429, 2014.

Nishimura Y, Perlmutter SI, Eaton RW, Fetz EE. Spike-timing-dependent plasticity in primate corticospinal connections induced during free behavior. *Neuron* 80: 1301–1309, 2013.

Nitsche MA, Boggio PS, Fregni F, Pascual-Leone A. Treatment of depression with transcranial direct current stimulation (tDCS): a review. *Exp Neurol* 219: 14–19, 2009.

Nitsche MA, Paulus W. Excitability changes induced in the human motor cortex by weak transcranial direct current stimulation. *J Physiol* 527: 633–639, 2000.

Pfurtscheller G and Lopes da Silva FH. Event-related EEG/MEG synchronization and desynchronization: basic principles. *Clin Neurophysiol* 110: 1842–1857, 1999.

Rahman A, Reato D, Arlotti M, Gasca F, Datta A, Parra LC, Bikson M. Cellular effects of acute direct current stimulation: somatic and synaptic terminal effects. *J Physiol* 591: 2563–2578, 2013.

Reed WR, Shum-Siu A, Whelan A, Onifer SM, Magnuson DS. Anterograde labeling of ventrolateral funiculus pathways with spinal enlargement connections in the adult rat spinal cord. *Brain Res* 1302: 76–84, 2009.

Sanes JN, Suner S, Lando JF, Donoghue JP. Rapid reorganization of adult rat motor cortex somatic representation patterns after motor nerve injury. *Proc Natl Acad Sci USA* 85: 2003–2007, 1988.

Shiozawa P, da Silva ME, Cordeiro Q, Fregni F, Brunoni AR. Transcranial direct current stimulation (tDCS) for the treatment of persistent visual and auditory hallucinations in schizophrenia: a case study. *Brain Stimul* 6: 831–833, 2013.

Song W, Martin JH. Patterned motor cortex stimulation can be potentiated by spinal cathodal DC stimulation to harness corticospinal system plasticity in the intact rat. *Soc Neurosc Abst* 2013.

Stagg CJ, Nitsche MA. Physiological basis of transcranial direct current stimulation. *Neuroscientist* 17: 37–53, 2011.

Starkey ML, Bleul C, Zorner B, Lindau NT, Mueggler T, Rudin M, Schwab ME. Back seat driving: hindlimb corticospinal neurons assume forelimb control following ischaemic stroke. *Brain* 135: 3265–3281, 2012.

Tan AM, Chakrabarty S, Kimura H, Martin JH. Selective corticospinal tract injury in the rat induces primary afferent fiber sprouting in the spinal cord and hyperreflexia. *J Neurosci* 32: 12896–12908, 2012.

Toshev PK, Guleyupoglu B, Bikson M. Informing dose design by modeling transcutaneous spinal direct current stimulation. *Clin Neurophysiol* 125: 2147–2149, 2014.

Winkler T, Hering P, Straube A. Spinal DC stimulation in humans modulates post-activation depression of the H-reflex depending on current polarity. *Clin Neurophysiol* 121: 957–961, 2010.